International Journal of
Metallurgical & Materials Engineering
Research Article Open Access

Novel Synthesis of Nanocrystalline Nickel Dispersed with Nano-size WO_3 Particles by Electrodeposition

Yushi Kato[1], Hiroshi Fujiwara[1], Hiroyuki Miyamoto[1*] and Takuya Goto[2]

[1]*Department of Mechanical Engineering, Doshisha University, 1-3 Miyakodani, Tatara, Kyotanabe, Kyoto 610-0321, Japan*
[2]*Department of Environmental System Engineering, Doshisha University, 1-3 Miyakodani, Tatara, Kyotanabe, Kyoto 610-0321, Japan*

Abstract

Bulk nanocrystalline nickel dispersed homogenously with nano-scale hard WO_3 particles has been successfully synthesized by a novel synthesis using electrodeposition. In this synthesis, ionized WO_4^{2-} molecules in an electrolyte were transformed into WO_3 particles and embedded into a nanocrystalline nickel matrix during electrodeposition by controlling the pH and potential of the electrode. The effect of the presence of nano-size oxide dispersions on the strength and thermal stability of nanocrystalline structures was demonstrated. This is indeed a new class of bulk nanocrystalline metals in that nano-scale second-phase particles are not reactive precipitate from the solute-supersaturated matrix, but are stable oxide particles resistant to the so-called Ostwald ripening. In this regard, future optimization of this synthesis have potential to realize nanocrystalline metals with record-high strength and thermal stability, superior to their precipitates- or solutes-stabilized counterparts.

Publication History:
Received: February 17, 2015
Accepted: April 04, 2015
Published: April 06, 2015

Keywords:

Electrodeposition, Nanocrystalline metal, Grain boundary strengthening, Orowan strengthening, Thermal stability

Introduction

Bulk nanocrystalline metallic materials have great strength and are promising materials for future structural applications. The possibility of additionally strengthening and enhancing the thermal stability of nanocrystalline metals by fine dispersions or precipitation is of increasing interest [1-10]. For example, additive strengthening by Orowan-type dislocation-particle interaction and the Hall-Petch effect in nanocrystalline materials have been discussed [1]. Particle dispersions or precipitates to pin grain boundaries are common kinetic approaches to stabilizing structures. According to classical Zener drag theory, the stabilized grain size, d, is given by $d = 0.66\varphi/f$, where φ is the particle size, and f is the volume fraction [11]. This means that very fine particles of about 4 nanometers are required to disperse homogeneously in order to stabilize nanocrystalline structures with a grain size of 50 nm (if the volume fraction f is 0.05). Such finely dispersed nanocrystalline metals have been very difficult to synthesize or fabricate by conventional methods. Solute-supersaturated ultrafine-grained aluminum alloys fabricated by severe plastic deformation, such as ECAP, have been stabilized by subsequent aging treatment where fine precipitates pin the grain boundaries [12,13]. However, one cannot avoid Ostwald ripening of the precipitate and a certain amount of grain growth during the ageing treatment. In the consolidation of mixed powders by mechanical alloying or ball-milling, fine particles tend to aggregate during the mixing process [14,15]. This trend becomes stronger with decreasing powder size due to the greater surface energy. Another method of synthesizing bulk nanocrystalline metals is electrodeposition, which is, from a synthesis point of view, one of the oldest methods used to produce nanostructured materials [16, 17]. Nanocrystalline metals dispersed with hard particles have generally been plated using an electrolyte with suspended hard particles such as SiC [18], Al_2O_3 [19], TiO_2 [20], and SiO_2 [21]. Similarly, particle size has been limited to dimensions larger than several microns in order to avoid particle agglomeration during the synthesizing.

During an effort to synthesize nanocrystalline nickel with very fine dispersed particles, the authors discovered that WO3 particles suspended in an electrolyte were fragmented into finer particles accompanying phase transition from a monoclinic to a tetragonal structure during electrodeposition [22,23]. The phenomenon has been successfully applied to synthesize bulk nanocrystalline metals with dispersed nano-size particles. However, the agglomeration could not be completely avoided, and the effect of nano-scale WO_3 particles on the further strengthening and thermal stability of the nanocrystalline matrix was limited.

In the current study, a novel new approach is proposed, wherein ionized WO_4^{2-} molecules were oxidized into nano-scale WO_3 particles, and then embedded homogeneously in nanocrystalline Ni during electrochemical reaction. If a new class of bulk nanocrystalline metals dispersed with stable nano-scale oxide particles having a size smaller than grain size could be obtained, it may have higher strength and thermal stability than the so-called heat-hardened nanocrystalline materials with reactive precipitates, since oxide particles have higher resistance to Ostwald ripening. In this study, the possibility of further strengthening and stabilizing structures by nano-size particles in a nanocrystalline regime was examined.

Experimental

Electrodeposition

Dispersed nanocrystalline nickel was plated by electrodeposition in a solution with a chemical composition as is shown in Table 1. Na_2WO_4 is considered to be electrolyzed into Na^+ and WO_4^{2-} in the solution. It was added to supply ionized WO_4^{2-} to the maximum of 20 *g/l*, and was intended to transform into WO_3 by a chemical reaction, as will be discussed later. Deposition was carried out using a DC plating power supply (Matsusada, PLE36-3) at a bath temperature of 50°C under a potential of -0.2 VSHE. pH was controlled between 4 and 5. During deposition, the plating bath was stirred by a magnetic stirrer with a rotation speed of 360 rpm. A rectangular AISI304 and

***Corresponding Author:** Dr. Hiroyuki Miyamoto, Department of Mechanical Engineering, Doshisha University, 1-3 Miyakodani, Tatara, Kyotanabe, Kyoto 610-0321, Japan; E-mail: hmiyamot@mail.doshisha.ac.jp

Citation: Kato Y, Fujiwara H, Miyamoto H, Goto T (2015) Novel Synthesis of Nanocrystalline Nickel Dispersed with Nano-size WO_3 Particles by Electrodeposition. Int J Metall Mater Eng 1: 102. doi: http://dx.doi.org/10.15344/2455-2372/2015/102

nickel plates with an area of 30 cm^2 were used as the cathode and anode electrodes, respectively. The depositions were carried out with a current density of 150 mA/cm^2 for three hours in order for the final thickness of the deposits to be approximately 0.1 mm.

$Ni(SO_3NH_3)_2.4H_2O$[g/l]	500
$NiCl_2.6H_2O$ [g/l]	10
H_3BO_3 [g/l]	30
$C_7H_5NO_3S$ [g/l]	2
$Na_2WO_4.2H_2O$ [g/l]	1-20

Table 1: Chemical composition of the electrolyte.

Characterization

Microstructures of the deposits were examined by transmission electron microscopy of a field-emission type, equipped with energy dispersion spectroscopy (FE-TEM with EDS, JEOL JSM 2100F). Samples were prepared for TEM by electropolishing with a solution of CH_3OH (75 %), CH_3COOH (15 %) and $HClO_4$ (10 %) at -30°C at a voltage of 15 V, using a Struers Tenupol-5 electropolishing apparatus. X-ray diffraction (XRD) analysis was performed on a Rigaku RINT2500 X-ray diffractometer using Co-Kα radiation. Microhardness was measured by a Vickers microindenter (Shimadzu HMV) on a cross section of the deposits, using a load of 980 mN applied for 20 s.

Results and Discussion

Figure 1 shows the relation between the amount of Na_2WO_4 in the electrolyte and W content in the electrodeposited plane, analyzed by ICP. The W content in the electrodeposits increased linearly with the amount of Na_2WO_4 in the electrolyte.excited by exerting an impulse at the middle of the length of the beam.

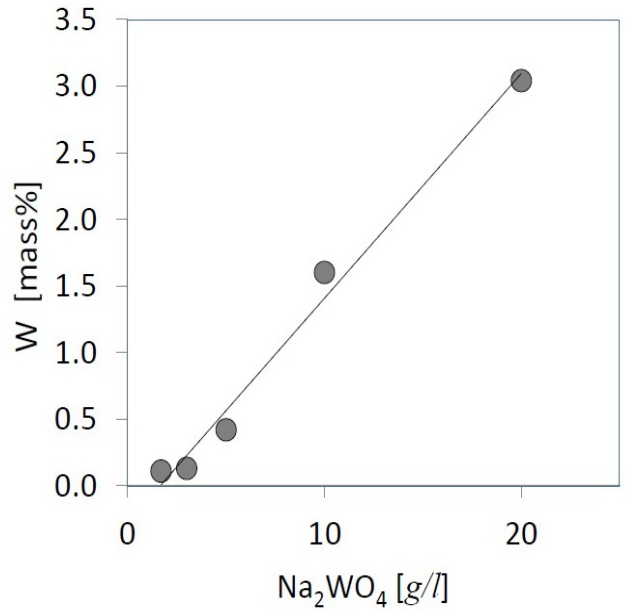

Figure 1: Relation between tungsten amount in electrodeposits and the amount of Na_2WO_4 in electrolyte.

Figure 2 shows TEM micrographs of as-electrodeposited microstructures. As shown in the bright-field image in Figure 2a, a nanocrystalline structure was formed in the as-electrodeposited state

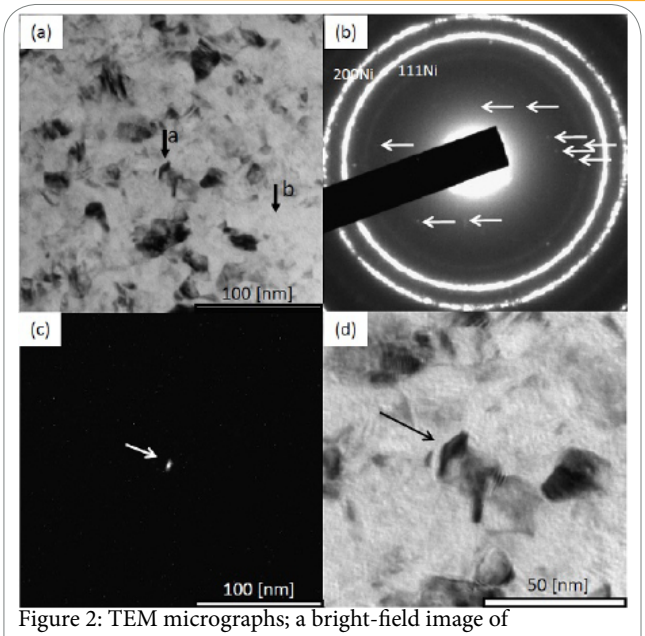

Figure 2: TEM micrographs; a bright-field image of nanocrystalline Ni-WO_3, b diffraction pattern of both Ni and WO_3. Arrows indicate diffraction spots identified as tetragonal WO_3, c dark-field image of the same area activated by 110 point indicated by the arrow in Figure 2b,2d bright-field image in higher magnification of marked area of c.

with an average grain size of 16 nm. Figure 2b shows a selected area diffraction pattern (SADP) of the same area in Figure 2a. One can observe several weaker spots inside (111) spots of nickel. Most of these spots correspond with those of tetragonal WO_3 structures, as indicated by the arrows. A dark-field image activated by a marked spot of WO_3 is shown in Figure 2c. Most importantly, very fine dispersions, comparable with the grain size of nickel matrix on the order of several nanometers, were recognized as shown in Figure 2c. One of the activated areas marked in the figure was observed by bright-field image in higher magnification as shown in Figure 2d, which indicates that the activated area is a single particle, not a grain or part of a particle. A nano-size dispersion inside a grain shown in the bright-field image (Figure 2a) has W and O elements, as indicated by EDS spot analysis equipped with FE-TEM (Figure 3a). This corroborates the facts that these particles are indeed tungsten oxide. On the other hand, those two elements were not detected in the matrix, indicating that they are not in a state of solid-solution. From several TEM observations, the average particles size was estimated to be 16 nm. The crystal structure of WO_3 could not be identified by XRD because the volume fraction and particle size were not large enough for XRD to detect them. WO_3 is known to take on many polymorphs and take several crystal structures. According to Boulova and Lucazeau [24], monoclinic or orthorhombic WO_3 particles transform into tetragonal structures when exposed to temperatures above 700K, when the particle size is 16 nm. During electrodeposition, it is possible that the plate of the surface rises above this temperature locally by the discharge of electricity. In our previous study [22,23], original WO_3 particles suspended in the electrolyte were monoclinic, but were identified as tetragonal structures in the electrodeposits by XRD and TEM.

Mechanism of WO_3 precipitation

According to the W-H_2O diagram shown in Figure 4, electrolyzed WO_4^{2-} ion is stable at the plating potential of -0.2 VSHE at a pH value

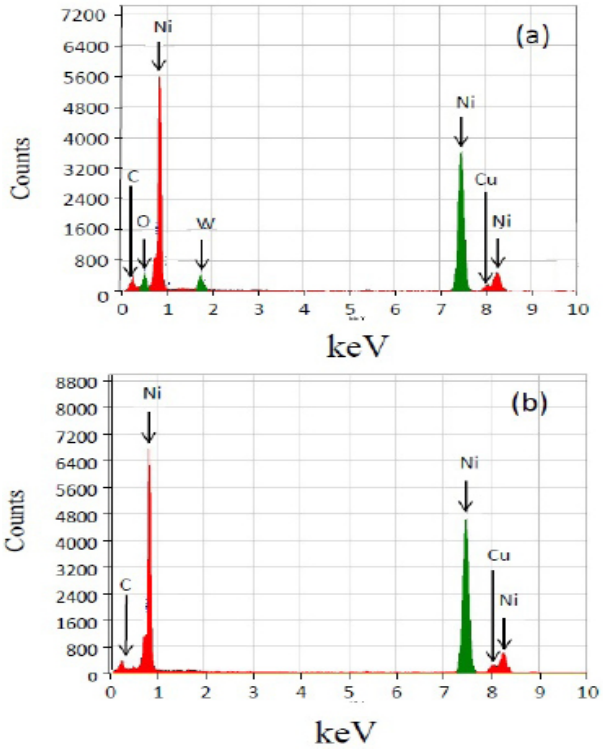

Figure 3: EDS spectrum by spot analysis on the particle indicated by arrow a, and b the area indicated by arrow b.

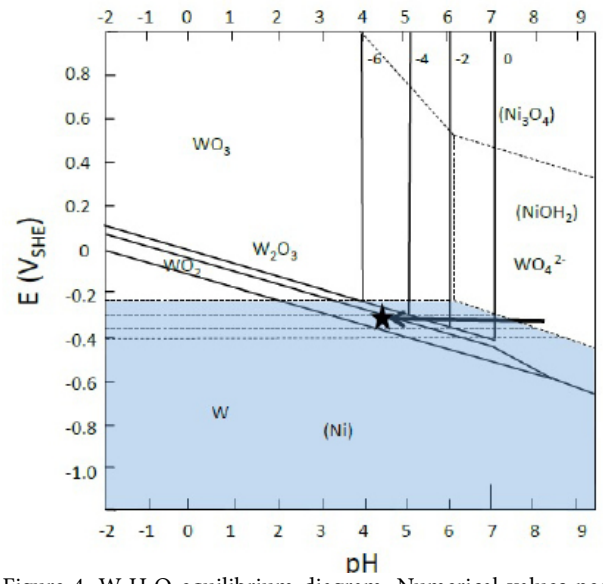

Figure 4: W-H_2O equilibrium diagram. Numerical values near vertical dotted lines indicate activity of WO_4^{2-}.

higher than 7. However, with pH lower than 4, insoluble WO_3 becomes stable by the following reaction:

$$WO_4^{2-} + 2H^+ \rightarrow WO_3 + H_2O$$

In Figure 4, the value with the vertical dotted lines indicates the activity of WO_4^{2-}, X, as expressed by:

$$\log X = -14.05 + 2pH$$

In the present experiment, pH=4.7 gives $X = 10^{-4.6} = 2.2\times10^{-8}$ mol/kg, and is essentially negligible. It means that almost all WO_4^{2-} transformed to WO_3 particles. It is therefore considered that single WO_3 molecules formed in the above reaction agglomerated and formed particles before being embedded into the plate. Since the delineating lines between WO_3, W_2O_5 and WO_2 are very close, reduction reaction from WO_3 to W_2O_5 and WO_2 may occur during electrodeposition.

Effect of dispersions on hardness of nanocrystalline Ni

Vickers hardness is plotted as a function of tungsten contents as shown in Figure 5. The hardness increased linearly with tungsten contents. This hardening is apparently caused by the presence of WO_3 particles. The data synthesized in the electrolyte of W=3 *g/l* are plotted as a function of grain size, as shown in Figure 6. Data of pure electrodeposited nanocrystalline Ni reported by El-Sherik [25] are also shown for comparison. The term "As" indicates as-electrodeposited

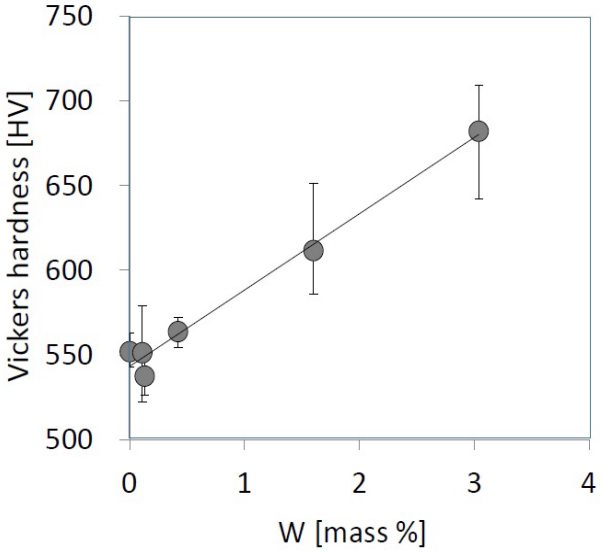

Figure 5: Relation between Vickers hardness and tungsten content in electrodeposits.

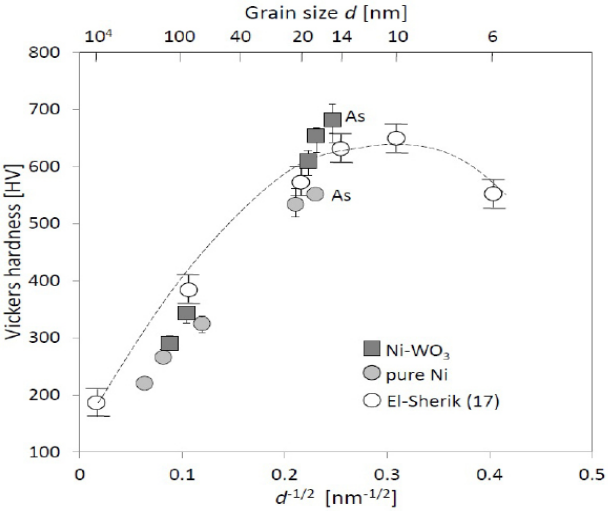

Figure 6: Variation of Vickers hardness of nanocrystalline electrodeposits as a function of grain size.

data for pure Ni and Ni-WO_3. The other plots with larger grain sizes were obtained by the subsequent annealing aiming for grain growth, as will be discussed in the next section. According to our data, the hardness of Ni-WO_3 with an average grain size of 16 nm is approximately 680. In view of a possible change in the dominant deformation mechanism from conventional dislocation slip to deformation mediated by grain boundaries, additional hardening by WO_3 particles is of interest. Thus, as was performed in the previous report [22], the result was compared with the theoretical strengthening by classical dislocation-pinning. According to the Orowan dislocation bowing model [26], yield stress σOR can be described as:

$$\sigma_{OR} = \frac{2mGb}{1.18 \times 4\pi(\lambda - \phi)} \ln\left(\frac{\phi}{2b}\right)$$

where m is the Taylor factor, G is the shear modulus of nickel matrix (75 GPa), b is the magnitude of the Burgers vector (2.49 Å for nickel), λ is the average particle center-to-center distance, and φ is the particle diameter [1]. Since the hardness H(MPa) is related to the tensile yield stress by $H=3\sigma y$, the increase in hardness, ΔH, which is related with the Orowan mechanism, can be rewritten as $\Delta HOR=3\sigma$OR. If one supposes that all of W analyzed by ICP, namely 3.0 mass %, is in the form of WO_3, the volume fraction of WO_3, f will be about 4.7 %. Mean inter-particle spacing λ is given by λ= $(4\pi/3f)1/3\ \varphi/2$. By substituting φ =17 nm in the equation, λ = 28 nm, which is not very different from the TEM observation. Supposing that grain orientations are random (m=3), the hardness increase will be ΔH_{OR} =330 HV, which is higher than the experimental result (ΔH~80 HV). The discrepancy may be due to several factors. The most important one is that as the grain size falls below around 50 nm, a variety of other deformation mechanisms can operate. Grain boundaries play a more dominant role in plastic deformation, acting as the source or sink of dislocations [27-31], or grain boundary siding by enhanced Coble diffusion [32-35]. Such a shift of deformation mode is in many cases reflected in the reduced slope of the Hall-Petch relationship, as is also shown in Figure 6, for pure nanocrystalline nickel with a grain size ranging from 20 to 50 nm [25]. The less dominant role of conventional dislocation slip may be the cause of less hardening than that predicted by Orowan theory. The second cause of the discrepancy is that the average particle size is comparable with the grain size of Ni matrix. Therefore, the density of particles inside the Ni grain is essentially less than that predicted above. The factor that controls particle size in the electrodeposition is still unknown, but if one can make it smaller than the matrix grain size, higher strength could be expected. A further study is now being undertaken.

Thermal stability

Vickers hardness and average grain size as a function of the heating temperature of post-electrodeposition annealing is shown in Figure 7. Pure nanocrystalline nickel started to decrease drastically at a temperature higher than 200°C, while Ni-WO_3 did so at temperatures higher than 300°C, almost 100°C higher than pure Ni electrodeposit. Correspondingly, grain size started to grow at 200°C and 300°C in pure Ni and Ni-WO_3, respectively. WO_3 is a very stable particle, and is hard to grow during aging treatment. This fine and stable particle is expected to pin grain boundaries by Zener pinning effect for a much longer time than that in the other age-hardenable alloys, such as Al-Cu systems. The stabilized grain size, namely, the Zener limit, Dz is expressed by

$$Dz = \frac{4r}{3f}$$

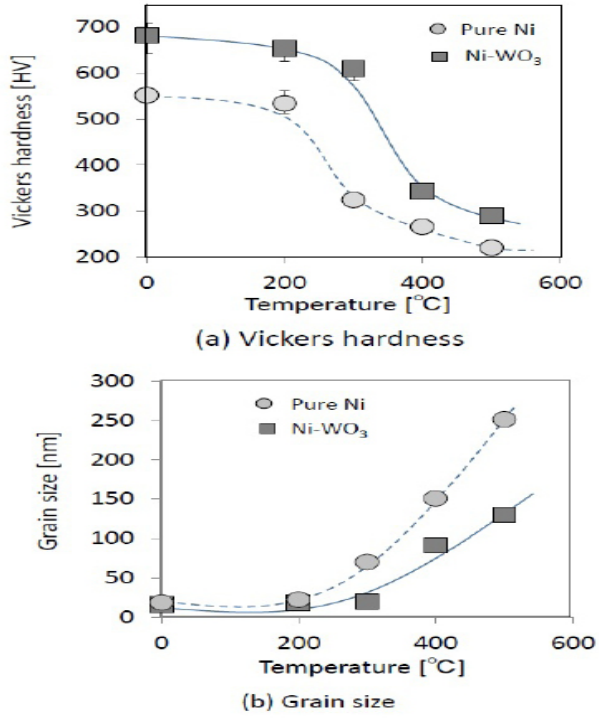

Figure 7: Influence of annealing temperature on a Vickers hardness, and b grain size after annealing for 40 minutes.

Where, f is the volume fraction of the particles, r is the diameter of the particles and is equal to $\varphi/2$. Supposing that all the W atoms in the matrix are in the form of WO_3, and r is 8 nm, then Dz = 210 nm. After annealing for 40 minutes at 500°C, the average grain size was about 130 nm, which is not far from the Zener limit. The pinning effect is more apparent when one examines the change in hardness after the various heating times. The results at 300°C are shown in Figure 8.

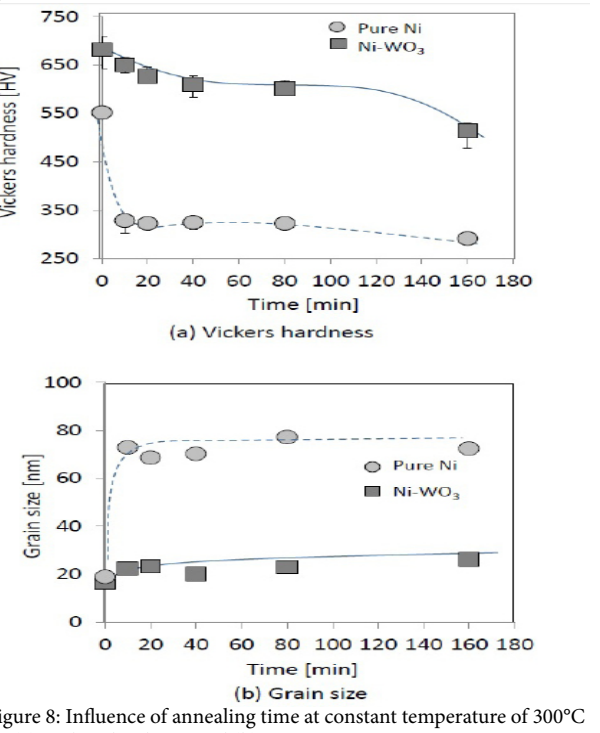

Figure 8: Influence of annealing time at constant temperature of 300°C on (a) Vickers hardness, and (b) grain size.

Hardness decreased in less than 20 minutes in pure nanocrystalline Ni, and its thermal stability was lower than that of nanocrystalline Ni-WO_3, where both were relatively constant for at least 100 minutes.

Conclusion

A nanocrystalline nickel plate dispersed with nano-size WO3 particles on the order of 10 nm was synthesized by electrodeposition, where electrolyzed WO_4^{2-} were transformed to WO_3 particles by pH and potential control, and embedded into a nanocrystalline electrodeposited Ni matrix. Further hardening was confirmed in comparison with nanocrystalline pure nickel having the same grain size, but its increment was less than that predicted by classical Orowan-type hardening theory of particle-dislocation interaction. The discrepancy may be associated with the comparable size of grain and particles, and a different dominant deformation mode which operates in a nanocrystalline regime. Enhanced thermal stability was also demonstrated. Further study is being undertaken to improve the current synthesis for higher strength and thermal stability.

Competing Interests

The authors declare that they have no competing interests.

Author Contributions

All the authors substantially contributed to the study conception and design as well as the acquisition and interpretation of the data and drafting the manuscript.

Funding

This work is financially supported by Grant-in-Aid for Scientific Research on Innovative Areas “Bulk nano metals,” MEXT Japan.

Acknowledgements

The authors gratefully acknowledge Professor Uwe Erb of the University of Toronto and Associate Professor Atsutomo Nakamura of Osaka City University for their helpful discussion. The authors would like to express their sincere gratitude to Professor Masaki Kato of Doshisha University for his valuable comments.

References

1. Morris DG, Morris MA (1991) Microstructure and strength of nanocrystalline copper alloy prepared by mechanical alloying. Acta Metallurgica et Materialia 39: 1763-1770.
2. Scattergood RO, Koch CC, Murty KL, Brenner D (2008) Strengthening mechanisms in nanocrystalline alloys. Mater Sci Eng A 493: 3-11.
3. Rajulapati KV, Scattergood RO, Murty KL, Horita Z, Langdon TG, Koch CC (2008) Mechanical properties of bulk nanocrystalline aluminum-tungsten alloys. Metall Mater Trans A 39:2528-2534.
4. Han BQ, Mohamed FA, Lavernia EJ (2003) Tensile behavior of bulk nanostructured and ultrafine grained aluminum alloys. J Mater Sci 38:3319-3324.
5. Srinivasan D, Corderman R, Subramanian PR (2006) Strengthening mechanisms (via hardness analysis) in nanocrystalline NiCr with nanoscaled Y2O3 and Al2O3 dispersoids. Mater Sci Eng A 416:211-218.
6. Shao I, Vereecken PM, Chien CL, Searson PC, Cammarata RC (2002) Synthesis and characterization of particle-reinforced Ni/Al2O3 nanocomposites. J Mater Res 17: 1412-1418.
7. Hou F, Wang W, Guo H (2006) Effect of the dispersibility of ZrO2 nanoparticles in Ni-ZrO2 electroplated nanocomposite coatings on the mechanical properties of nanocomposite coatings. Appl Surf Sci 252: 3812-3817.
8. Klement U, Erb U, El-Sherik AM, Aust KT (1995) Thermal stability of nanocrystalline Ni. Mater Sci Eng 20: 3177-186.
9. Koch CC, Scattergood RO, Darling KA, Semones JE (2008) Stabilization of nanocrystalline grain sizes by solute additions. J Mater Sci 43: 7264-7272.
10. Wilde G, Rosner H (2007) Stability aspects of bulk nanostructured metals and composites. J Mater Sci 42 :1772-1781.
11. Zener C (1948) Trans AIME 15:175-177
12. Horita Z, Ohashi K, Fujita T, Kaneko Y, Langdon TG (2005) Achieving high strength and high ductility in precipitated-hardened alloys. Adv Mater 17: 1599-1602.
13. Kim JK, Jeong HG, Hong SI, Kim YS, Kim WJ (2001) Effect of aging treatment on heavily deformed microstructure of a 6061 aluminum alloy after equal channel angular pressing. Scr Mater 45: 901-907.
14. Li Y, Zhao YH, Ortalan V, Liu W, Zhang ZH, et al. (2009) Investigation of aluminum-based nanocomposites with ultra-high strength. Mater Sci Eng A 527: 305-316.
15. Balazsi C, Gillemot F, Horvath M, Weber F, Balazsi K, et al. (2011) Preparation and structural investigation of nanostructured oxide dispersed strengthened steels. J Mater Sci 46:4598-4605.
16. Erb U (1995) Electrodeposited Nanocrystals-Synthesis, Structure, Properties and Future Applications. Can Metall Q 34:275-280.
17. El-Sherik AM, Erb U (1995) Synthesis of bulk nanocrystalline nickel by pulsed electrodeposition. J Mater Sci 30:5743-5749.
18. Hu F, Chan KC, Qu NS (2007) Effect of magnetic field on electrocodeposition behavior of Ni-SiC composite. J Sol Stat Electrochem 11: 267-272.
19. Jung A, Natter H, Hempelmann R, Lach E (2009) Nanocrystalline alumina dispersed in nanocrystalline nickel: enhanced mechanical properties. J Mater Sci 44:2725-2735.
20. Li J, Sun Y, Sun X, Qiao J (2005) Mechanical and corrosion-resistance performance of electrodeposited titania-nickel nanocomposite coating. Surf Coat Technol 192: 331-335.
21. Miyamoto H, Ueda K, Uenoya T (2010) Mechanical properties of electrodeposited Ni-SiO2 nanocomposite. Mater Sci For 654-656:1162-1165.
22. Miyamoto H, Takehara S, Uenoya T, Fujiwara H, Goto T (2012) Nanocrystalline nickel dispersed with nano-size WO3 particles synthesized by electrodeposition. J Mater Sci 47:4798-4804.
23. Miyamoto H, Takehara S, Uenoya T, Fujiwara H, Goto T (2012) Electrodeposited nanocrystalline nickel dispersed with nano-size WO3 particles. Mater Trans 53: 1026-1028.
24. Boulova M, Lucazeau G (2002) Crystallite nanosize effect on the structural transitions of WO3 studied by Raman spectroscopy. J Solid State Chem. 167: 425-434.
25. El-Sherik AM, Erb U, Palumbo G, Aust KT (1992) Deviations from Hall-Petch behavior in as-prepared nanocrystalline nickel. Scr Metall Mater 27:1185-1188.
26. Kocks UF (1966) A statistical theory of flow stress and work-hardening. Phil Mag A 13:541-566.
27. Kumar KS, Vanswygenhoven H, Suresh S (2003) Mechanical behavior of nanocrystalline metals and alloys. Acta Mater 51: 5743-5774.
28. Chen M, Ma E, Hemker KJ, Sheng H, Wang Y, et al. (2003) Deformation twinning in nanocrystalline aluminum. Science 300: 1275-1277.
29. Liao XZ, Zhao YH, Srinivasan R, Zhu YT, Valiev R, Gunderov DV (2004) Deformation twinning in nanocrystalline copper at room temperature and low strain rate. Appl Phys Lett 84: 592-594.
30. Zhu YT, Liao XZ (2004) Nanostructured Metals Retaining ductility. Nat Mater 3: 351-352.
31. Wu X, Ma E, Zhu YT (2007) Deformation defects in nanocrystalline nickel. J Mater Sci 42:1427-1432.
32. Chokshi AH, Rosen A, Karch J, Gleiter H (1989) On the validity of the hall-petch relationship in nanocrystalline materials. Scr Metall 23: 1679-1683.

33. Chinh NQ, Szommer P, Horita Z, Langdon TG (2006) Experimental evidence for grain boundary sliding in ultrafine grained aluminum processed by severe plastic deformation. Adv Mater 18:34-39.

34. Wang N, Wang ZR, Aust KT, Erb U (1997) Room temperature creep behavior of nanocrystalline nickel produced by an electrodeposition technique. Mater Sci Eng A 237:150-158.

35. Trusov LI, Khvostantseva TP, Solovev VA, Melnikova VA (1995) Low temperature stress relaxation of nanocrytalline nickel. J Mater Sci 30: 2956-2961.